Physica B 579 (2020) 411896

Contents lists available at ScienceDirect

Physica B: Physics of Condensed Matter

journal homepage: http://www.elsevier.com/locate/physb

X-ray derived experimental charge density distribution in two isostructural oxyfluorotellurates, $FeTeO_3F$ and $GaTeO_3F$

K. Sujatha [a,b], S. Israel [b,*], C. Anzline [a,b]

[a] Research Scholar, Mother Teresa Women's University, Kodaikanal, 624 102, Tamil Nadu, India
[b] Research and Post Graduate Department of Physics, The American College, Madurai, 625 002, India

ARTICLE INFO

Keywords:
Charge density
Multipole model
MEM model
Bond critical points
Debye-waller factors
Zero flux atomic basins

ABSTRACT

The electronic structure and bonding features of two isostructural oxyfluorotellurates, $FeTeO_3F$ and $GaTeO_3F$ have been thoroughly investigated by precise experimental charge density distribution evolved from single crystal X-ray diffraction experiments using multipole and MEM models of charge density. The topology of the charge density is explored and the ligand atoms endorsing different bonding characteristics at different symmetries are well documented by studying (3,-1) bond critical points. Existences of mixed ionic and covalent nature of bondings are clearly evident in the two systems and mapped. Debye-Waller factors and charge integration over zero flux atomic basins reveal that oxyfluorotellurate of gallium is a hard molecule.

1. Introduction

Contributions to and success stories of Crystallography, a persistent hot topic of research, has been so far relied on X ray diffraction. Though X ray crystallography and its methods have continued to develop soon after the discovery of X ray diffraction in 1912 [1,2], a very mature field, charge density, marks the dawn of modern crystallography, since it can provide enhanced insight into several important properties of the materials through the elucidation of precise electronic structure of the materials and its bonding motifs [3,4]. The knowledge and ardent studies in charge density solves many basic problems related to the function of the materials and thus paves the way to optimize the behavior of the materials as 'future materials' for real applications [5].

Fervent research on oxyfluorides is actually driven by a quest to understand the union of two contrasting traits of mostly ionic metal fluorides and partly covalent metal oxides [6–13] rather than its myriad of electronic, magnetic and optical applications [10,11,13–21]. Perhaps, the properties of these materials which are deemed to be intermediary between the two limits of bonding character [10,13] and hence the confluence advantages of fluorides and favorable effects of oxides invites its applications [13,19,22]. Indeed, owing to the limited theoretical electron density studies on inorganic oxyfluorides [21], an apparent knowledge about the diverse bonding interactions in these captivating materials is strongly desired. Lately, the burgeoning field of oxyfluorides is the incorporation of a p-block element, comprising a stereochemically active or inactive lone pair electrons (such as Se^{4+}, Sn^{2+}, Sb^{3+}, Te^{4+}, Pb^{2+}, Bi^{3+} etc) [23–26] as a cation into the metal oxyfluorides. In these oxyfluorides, the presence of stereochemically active lone pair electrons gives rise to noncentrosymmetric (NCS) crystal structures with interesting functional properties including ferroelectricity, second harmonic generation (SHG), pyroelectricity and piezoelectricity [24–32] and topologically low dimensional crystal structures with intriguing physical properties such as magnetic frustration [24,26,27,33]. Nevertheless, in consequence of the difficulties in synthesis tactic [24–27], few works have ever been described about the inorganic metal or transition metal oxyfluorides in the M-L-O-F family, (M = Metal or Transition metal and L = p-block cation lone pair), (for instance, $Co_2SeO_3F_2$, $Co_2TeO_3F_2$, $FeSeO_3F$, $FeSbO_2F_2$, $FeTeO_3F$, FePbO2F, $Fe_5Bi_4O_{13}F$, $GaTeO_3F$, $In_3TeO_3F_7$, $InTe_2O_5F$, $InTeO_3F$, $ScTeO_3F$, $TiTeO_3F_2$, $V_2Te_2O_7F_2$, VBi_2O_5F, $YSeO_3F$, $Zn_3Sb_4O_6F_6$, to name just a few) [24–34]. In this regime, surprisingly, to date there have been no reports on charge density studies of these structurally complex and diverse compounds. Correlation of structure and physical properties of the materials requires an understanding of the bonding mechanisms involved. This invoked the inevitability of a well documented charge density research in the M-L-O-F family of compounds.

Literally, the term low dimensional compound refers to the arrangement of metal cation in the form of zero-dimensional clusters, one dimensional chains or two-dimensional layers [23,35]. From a structural viewpoint, the M-L-O-F compounds usually crystallize with

---

* Corresponding author.
E-mail address: israel.samuel@gmail.com (S. Israel).

https://doi.org/10.1016/j.physb.2019.411896
Received 19 August 2019; Received in revised form 24 October 2019; Accepted 18 November 2019

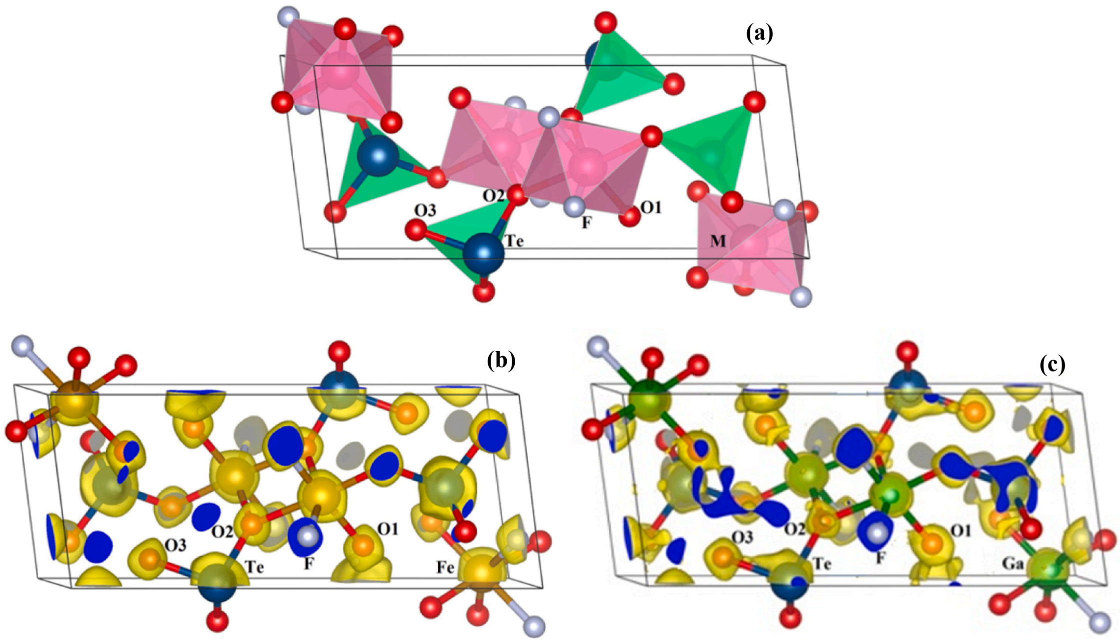

Fig. 1. (a). Isostructural unit cell of MLO_3F (M = Fe, Ga and L = Se, Te). 3- dimensional charge density distribution in (b) $FeTeO_3F$ and (c) $GaTeO_3F$ unit cell. The isosurface level is 0.8 e/Å^3.

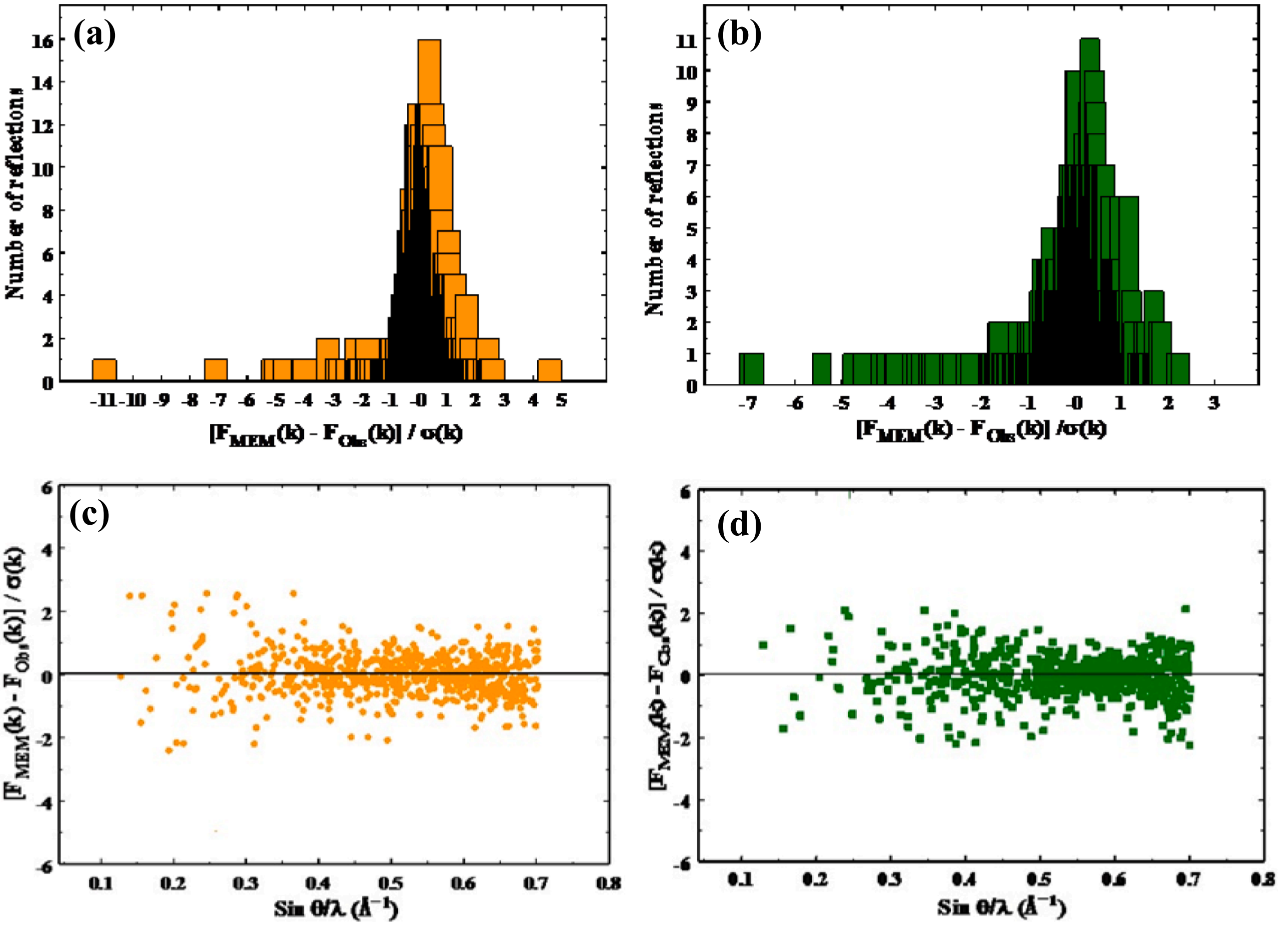

Fig. 2. Histogram of observed number of reflections of (a) $FeTeO_3F$ and (b) $GaTeO_3F$. Error distribution of the observations in reciprocal space of (c) $FeTeO_3F$ and (d) $GaTeO_3F$.

Table 1
Summary of least squares and MEM refinement.

Parameters	Structure refinement using least-squares procedure			
	$FeTeO_3F$		$GaTeO_3F$	
	Present work	[32]	Present work	[32]
a (Å)	5.0875 (15)	5.0667 (7)	5.0825 (21)	5.0625 (7)
b (Å)	5.0621 (15)	5.0550 (7)	4.9990 (10)	4.9873 (7)
c (Å)	12.3000 (8)	12.3975 (15)	12.1000 (9)	12.1662 (15)
β (degrees)	97.638 (10)	97.630 (13)	97.957 (10)	97.952 (13)
Cell Volume ($Å^3$)	314.7 (8)	314.72 (7)	304.2 (8)	304.22 (7)
Density (gm/cc)	5.2839	5.286	5.7690	5.771
$B_{Te}(Å^2)$	0.4849 (12)	–	0.3349 (4)	–
$B_M(Å^2)$	0.5008 (2)	–	0.3514 (11)	–
$B_F(Å^2)$	0.6475 (13)	–	0.4649 (7)	–
$B_O(Å^2)$	O1 - 0.6545 (21) O2 - 0.7856 (3) O3 - 0.8851 (17)	–	O1 - 0.5000 (9) O2 - 0.6731 (3) O3 - 0.6555 (5)	–
R_{obs} (%)	1.64	–	1.58	–
wR_{obs} (%)	1.43	–	2.23	–
GOF	0.89	–	0.91	–
	Charge density by MEM refinement			
Lagrange parameter	0.124000	–	0.050867	–
Number of cycles	277	–	394	–
Prior electron density (e/$Å^3$)	1.4108	–	1.5252	–
Resolution ($eÅ^{-3}$/pixel)	0.08	–	0.08	–
R_{obs} (%)	1.46	–	1.08	–
wR_{obs} (%)	1.73	–	1.39	–

Table 2
Core and valence populations derived from kappa refinements.

Molecules	Atoms	Parameters			
		P_C	P_V	κ	κ′
$FeTeO_3F$	Te	45.9613	5.0912	1.0222	1.0000
	Fe	24.0071	1.4454	1.0432	1.0000
	F	2.0000	7.2958	0.9763	1.0000
	O1	1.9969	6.5764	0.9695	1.0000
	O2	1.9854	6.8370	0.9535	1.0000
	O3	1.9972	6.6168	0.9582	1.0000
$GaTeO_3F$	Te	46.0491	4.6993	1.0149	1.0000
	Ga	27.9912	1.2602	1.0115	1.0000
	F	2.0036	7.3266	0.9789	1.0000
	O1	2.0104	6.0834	0.9880	1.0000
	O2	2.0117	6.5107	0.9700	1.0000
	O3	2.0135	6.6049	0.9574	1.0000

unusual structures [23,30,35] having reduced dimensionality which is endorsed by the existence of the stereochemically active lone pair cation acting as "chemical scissors" separating the coordination polyhedra around the metal cations from forming three dimensional networks [26,27]. Probably, the halide ions only bond to the metal cation and hence such scissors form as few bonds as possible [25]. The search of finding structurally related compounds in this wide structurally diverse area shows the way to the surveys of Shichao Hu and Mats Johnsson [26] describing the isostructural orthorhombic Copper (II) Oxyfluorotellurate (IV) and Copper (II) Oxyfluoroselenite (IV) solid systems with Pnma space group symmetry and Shichao Hu et al. [27] and Jean Paul Laval et al. [32] describing the isostructural monoclinic Iron (III) Oxyfluoroselenite (IV), Iron (III) Oxyfluorotellurate (IV) and Gallium (III) Oxyfluorotellurate (IV) solid systems with $P2_1/n$ space group symmetry. While these compounds have been the subject of some previous studies, except $FeTeO_3F$ and $GaTeO_3F$, for the other systems, the crystal structure and magnetic properties have been well described in detail. Concerning the former two molecules, only the crystal structure has been reported. Such state of affairs invoked the significance of an exploratory charge density research on these less explored oxyfluorotellurates, $FeTeO_3F$ and $GaTeO_3F$. To the best of our knowledge, the present work provides the first experimental charge density studies on the areas of both oxyfluorides and oxyfluorides comprising lone pair cations.

The isostructural unit cell of MLO_3F (M = Fe, Ga and L = Se, Te) (Fig. 1(a)) shows that each metal/transition metal cation, coordinated to three oxygen sites O1, O2 and O3, i.e. four oxygen atoms (one O1, two O2 and one O3 atoms), and two fluorine atoms of same site, exhibit a zigzag one dimensional chain like arrangement of MO_4F_2 octahedra alternately sharing the O–O and F–F edges and interconnected via LO3 trigonal pyramids, in which the lone pair cation L, is bonded to three oxygen ligands i.e. three oxygen sites viz. O1, O2 and O3 forming a one-sided asymmetric coordination. Tetrahedral LO_3E (E = stereochemically active lone pair electrons) distorted coordination has been observed in all the three compounds, in spite of a slight difference in size between SeO_3E and TeO_3E coordination [24]. Further, as mentioned earlier, there is lack of strong LF bonds and as a consequence, these phases assure high thermal and chemical stability [27,30,31]. With these fundamental structural details, this present study has been initiated with a hope to provide a further insight into the charge related and bonding properties of these oxyflurotellurates of iron and gallium.

2. Crystallization and X – ray data collection

The two above said chosen materials can be crystallized by the same method as accounted by Jean Paul Laval et al. [32]. The product, obtained from the slow evaporation of the mixture of $\frac{1}{2}$ Fe_2O_3: 4 TeO_2 dissolved in 40 % of hydrofluoric acid in a Teflon beaker at $180\,^{\circ}C$, when sealed in a platinum tube, subjected to the following heat treatment: ambient temperature rise at $500\,^{\circ}C$ ($5\,^{\circ}C$/min), kept stable for 4 days, slow descent at $400\,^{\circ}C$ ($0.05\,^{\circ}C$/min), kept stable for 10 h, and finally quenched with water, will yield light green crystals of $FeTeO_3F$. Similar procedure (except the ambient temperature rise is at $700\,^{\circ}C$ and the rate of decrease in temperature is $0.1\,^{\circ}C$/min), when followed, for a mixture of $\frac{1}{2}$ Ga_2O_3: 2 TeO_2, will yield colourless crystals of $GaTeO_3F$.

A Bruker Smart Apex CCD area detector using a graphite monochromated MoKα radiation (λ = 0.71073 Å) can be used to perform high resolution single crystal diffraction experiments. A complete set of reflection data, thus collected for both the samples is utilized for extensive charge density studies.

3. Refinement strategies

3.1. Structure refinement

The standard least-squares procedure by the full matrix method was adopted for refining the raw structure factors of both the data sets of $FeTeO_3F$ and $GaTeO_3F$ while incorporating the corrections for absorption [36] and extinction effects using a Zachariasen model [37] and for Thermal Diffuse Scattering parameters (TDS). According to this method, the quantity minimized is considered as,

$$D = \sum_{hkl} W_{hkl}\left(|F_O| - |F_C|\right)^2$$

where W_{hkl} is the weight to be assigned to an observation and F_O and F_C are the observed and calculated structure factors respectively.

3.2. Electron density estimation

The two more reliable models of electron density estimation, Maximum Entropy Method (MEM) and Multipole formalism, have been

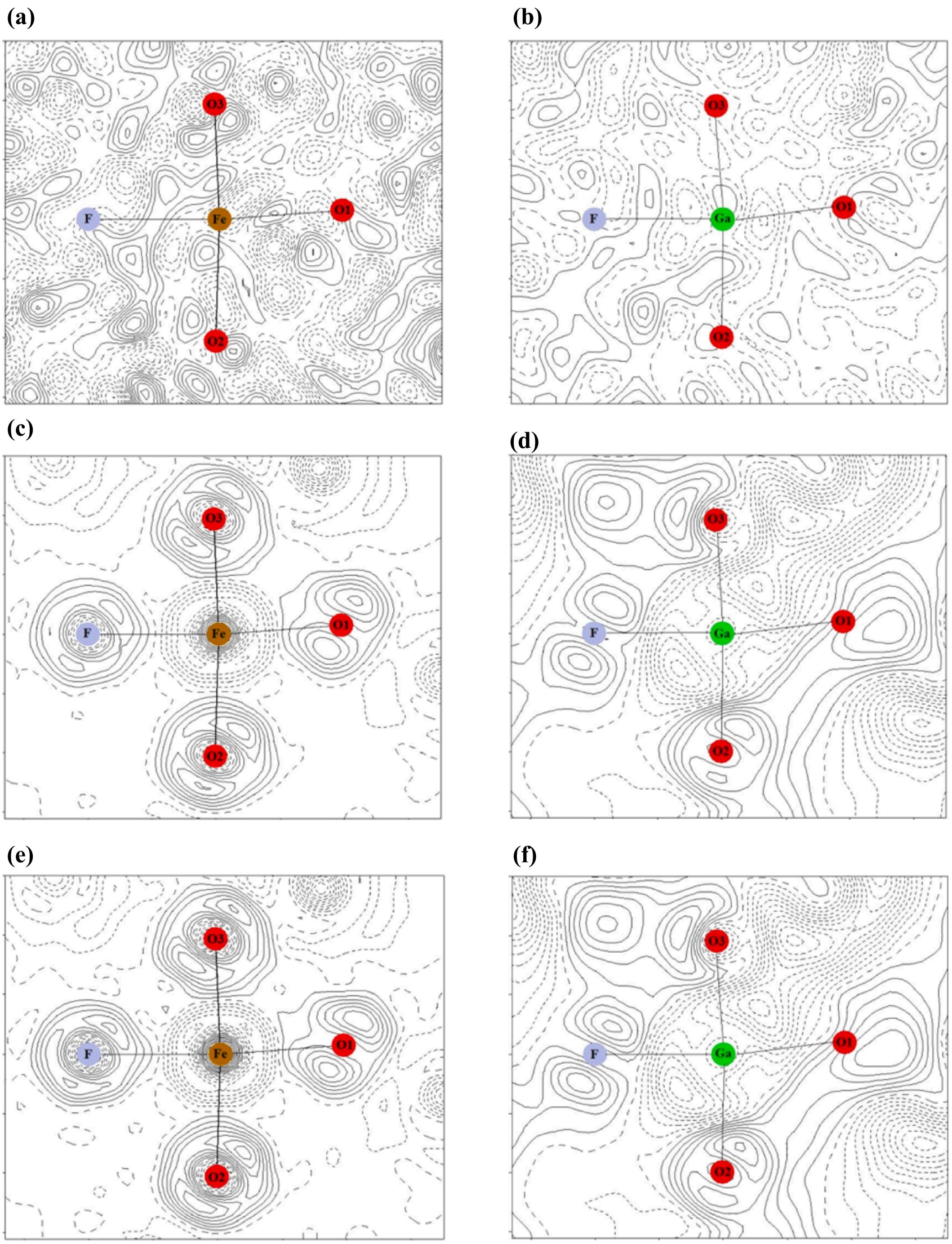

Fig. 3. Difference Fourier maps of (a) $FeTeO_3F$ and (b) $GaTeO_3F$, Dynamic deformation multipole density maps of (c) $FeTeO_3F$ and (d) $GaTeO_3F$ and Static deformation multipole density maps of (e) $FeTeO_3F$ and (f) $GaTeO_3F$. Negative contours are shown with dashed lines.

used to describe the precise distribution of density of charges in these materials.

3.2.1. MEM refinement

3.2.1.1. Theory. The maximum entropy method is one of the versatile statistical approach, proposed by Collins [38], to construct the appropriate density distribution even from a limited information obtained experimentally. The basic concept of this method, as proposed by Sakata and Sato [39], is to maximize the entropy in an iterative cycle at the ith pixel in a unit cell in terms of the assumed uniform prior density at that pixel until a weak constraint,

$$C = \frac{1}{N}\sum_{k}\frac{|F_{obs}\ (k) - F_{cal}(k)|^2}{\sigma^2}$$

that compares the observed ($F_{obs}\ (k)$) and calculated ($F_{cal}(k)$) structure factors, be inclined to 1. Here N denotes the number of reflections and σ denotes the standard deviation. Hence the resulting electron density is,

$$\rho_{MEM}(r_i) = \tau(r_i)\exp\left[\left(\frac{\lambda F_{000}}{N}\right)\sum[1/\sigma(k)]^2|F_{Obs}\ (k) - F_{Cal}(k)|\exp(-2\pi j\ k.r)\right]$$

where $\tau(\boldsymbol{r}_i)$ and F_{000} signify the prior electron density and the number of electrons in the unit cell correspondingly. When the Lagrange's

Table 3
Topological properties at the (3,-1) Bond Critical Points.

Bond Type	Molecules	Bond	Symmetry	MEM			Multipole	[32]	Tsirelson's classification of BCP, $\rho(r)$ (e/Å^3)		
				d (Å)	d_1 (Å)	d_2 (Å)	d (Å)	d (Å)	Ionic interactions	Intermediate interactions	Polar covalent interactions
Te–O	$FeTeO_3F$	Te – O1	Te – (x, y, z) O1 – (x, y, z) Fig. 4(a)	1.8910	1.1796	0.7114	1.8911	1.8840	–	–	1.3952
		Te – O2	Te – (x, y, z) O2 – (x, y, z) Fig. 4(a) &(b)	1.9684	1.2229	0.7455	1.9684	1.9040	–	0.6175	–
		Te – O3	Te – (x, y, z) O3 – (x, y, z) Fig. 4(b)	1.8961	1.1787	0.7174	1.8960	1.8700	–	0.3838	–
	$GaTeO_3F$	Te – O1	Te – (x, y, z) O1 – (x, y, z) Fig. 4(c)	1.8837	0.7667	1.1170	1.8840	1.8840	–	–	1.4201
		Te – O2	Te – (x, y, z) O2 – (x, y, z) Fig. 4(c)&(d)	1.9177	1.2046	0.7131	1.9178	1.9180	0.1467	–	–
		Te – O3	Te – (x, y, z) O3 – (x, y, z) Fig. 4(d)	1.9002	1.1875	0.7127	1.9002	1.8650	–	0.7273	–
M – O	$FeTeO_3F$	Fe – O1	Fe – (x, y, z) O1 – (-x+1/2, y+1/2, -z+1/2) Fig. 5(a)	1.9927	1.1526	0.8401	1.9930	1.9230	–	0.3317	–
		Fe – O2	Fe – (x, y, z) O2 – (x+1/2,- y+1/2, z+1/2) Fig. 5(a)	2.0477	1.2295	0.8182	2.0475	2.0540	–	0.3308	–
			Fe – (x, y, z) O2 – (-x+1/2, y+1/2, -z+1/2) Fig. 5(b)	1.9631	1.0654	0.8977	1.9628	1.9650	–	0.3232	–
		Fe – O3	Fe – (x, y, z) O3 – (x, y, z) Fig. 5(a)	1.9202	1.1210	0.7992	1.9202	1.9410	–	0.5722	–
	$GaTeO_3F$	Ga - O1	Ga – (x, y, z) O1 – (-x+1/2, y+1/2, -z+1/2) Fig. 5(c)	1.9054	0.9479	0.9575	1.9054	1.9180	–	0.7185	–
		Ga – O2	Ga – (x, y, z) O2 – (x+1/2,- y+1/2, z+1/2) Fig. 5(c)	2.0139	0.8343	1.1796	2.0138	1.9870	0.2552	–	–
			Ga – (x, y, z) O2 – (-x+1/2, y+1/2, -z+1/2) Fig. 5(d)	1.9638	1.0253	0.9385	1.9638	1.9230	0.1359	–	–
		Ga – O3	Ga – (x, y, z) O3 – (x, y, z) Fig. 5(c)	1.9087	0.9879	0.9208	1.9087	1.9110	–	0.4904	–
M – F	$FeTeO_3F$	Fe–F	Fe – (x, y, z) F – (-x, -y,- z) Fig. 5(a)	2.0089	1.0875	0.9214	2.0090	2.0400	0.2246	–	–
			Fe – (x, y, z) F – (x, y, z) Fig. 5(b)	1.9339	0.9619	0.9720	1.9339	1.9740	0.2224	–	–
	$GaTeO_3F$	Ga–F	Ga – (x, y, z) F – (-x, -y,- z) Fig. 5(c)	2.0651	0.8381	1.2270	2.0650	2.0090	–	0.4486	–
			Ga – (x, y, z) F – (x, y, z) Fig. 5(d)	1.9250	0.7446	1.1804	1.9250	1.9290	–	0.3939	–

multiplier λ, $\sigma(k)$ and $F_{Obs}(k)$ are given, $\rho(r_i)$ could be obtained, which is the desired MEM estimate.

3.2.1.2. Refinement. After the structural parameters have been successfully refined, the structure factors were used for the Collins [38] methodology of MEM estimation, with the assistance of the software package PRIMA [40,41]. Initially, the unit cells of FeTeO3F and $GaTeO_3F$ is divided so as to contain 64 × 64 x 156 pixels. At each of these pixels, the prior charge density is fixed uniformly as $F_{000}/a^3 = 1.4108$ e/Å^3 for $FeTeO_3F$ and 1.5252 e/Å^3 for $GaTeO_3F$ (F_{000} is the total number of electrons in the unit cell and a is the cell parameter). Lagrange parameter is duly elected so that, after a minimum number of iterations, the convergence criterion, C = 1 is achieved by maximizing the entropy. The visualization software package VESTA [42] is used to map the resultant density quantitatively.

3.2.2. Multipole refinement

3.2.2.1. Theory. The changes in the structure of the electron density due to aspherical expansion/contraction of atoms, while bonding, and to its thermal environment, and also the population parameters that correspond to the quantified charge involved in the bonding process can be determined by the modified model proposed by Hansen and Coppens [43], that provides an option to refine population parameters at various orbital levels. This model consists of a superposition of harmonically vibrating aspherical atomic density distributions:

$$\rho(r) = \sum_{k}^{atoms} \rho(r - r_k - u) \otimes t_k(u)$$

Here $t_k(u)$ indicates the Gaussian term and the symbol ⊗ stand for convolution. Each atomic density is then expressed as a series expansion in real harmonic functions through fourth – order (Y_{lm}).

$$\rho(r) = P_c\,\rho_{core}(r) + P_v\,\kappa^3\rho_{valence}(\kappa r) + \sum_{l=0}^{4} \kappa'^3 R_l(\kappa' r) + \sum_{m=-l}^{l} P_{lm} Y_{lm}\left(\frac{\vec{r}}{r}\right)$$

where P_c , P_v and P_{lm} are population coefficients and $R_l(\kappa' r)$ is the slater type radial function. Although, the functions ρ_{core} and $\rho_{valence}$ are selected as the Hartree – Fock (HF) densities of the free atoms normalized to one electron, the valence function is permitted to expand and contract by the adjustment of the variable radial parameters κ and κ'. Hence ρ_{core} and $\rho_{valence}$ are constructed from the canonical HF orbitals.

Table 4
Bond angles.

Bond angles (°)		$FeTeO_3F$			$GaTeO_3F$		
		Present work		[32]	Present work		[32]
		MEM	Multipole		MEM	Multipole	
O–Te – O	O1 – Te – O2	94.9938 (1)	94.9940 (1)	94.9900 (10)	94.9449 (0)	94.9450 (0)	94.8700 (10)
	O1 – Te – O3	93.5112 (2)	93.5112 (0)	93.5500 (10)	93.4520 (1)	93.4520 (0)	93.3100 (10)
	O2 – Te – O3	97.0296 (0)	97.0297 (0)	97.0500 (10)	95.9164 (0)	95.9165 (1)	95.9400 (9)
O – M – O	O1 – M – O2	95.9485 (0)	95.9485 (0)	95.9100 (10)	96.6166 (0)	96.6168 (0)	96.6200 (9)
		99.7979 (1)	99.8000 (0)	99.8100 (11)	101.4451 (0)	101.4451 (1)	101.5800 (10)
	O1 – M – O3	87.6897 (0)	87.6897 (0)	87.7100 (10)	87.3242 (2)	87.3242 (0)	87.2900 (9)
	O2 – M – O2	78.5839 (0)	78.5838 (1)	78.6500 (10)	78.4644 (1)	78.4644 (0)	78.4400 (9)
	O2 – M – O3	176.3254 (0)	176.3254 (0)	176.3500 (10)	176.0471 (0)	176.0470 (0)	176.0700 (9)
		100.3248 (2)	100.3248 (0)	100.3000 (10)	100.4947 (0)	100.4947 (1)	100.5100 (9)
O – M – F	O1 – M – F	172.5832 (0)	172.5832 (0)	172.6200 (10)	170.1160 (1)	170.1162 (2)	170.0500 (9)
		99.4598 (0)	99.4600 (1)	99.4700 (10)	97.5848 (0)	97.5850 (0)	97.4600 (9)
	O2 – M – F	88.6334 (0)	88.6334 (1)	88.6600 (9)	89.3185 (0)	89.3185 (0)	89.3900 (8)
		86.8046 (2)	86.8046 (2)	86.7500 (9)	87.4552 (2)	87.4552 (0)	87.3600 (9)
		85.2035 (0)	85.2033 (0)	85.1500 (9)	86.5510 (0)	86.5511 (1)	86.5500 (8)
		155.9400 (0)	155.9400 (0)	155.9300 (10)	156.9367 (0)	156.9367 (2)	156.9100 (8)
	O3 – M – F	87.8003 (0)	87.8003 (0)	87.7900 (9)	86.8213 (0)	86.8213 (0)	86.7700 (8)
		94.7268 (1)	94.7269 (1)	94.7400 (9)	93.2521 (0)	93.2521 (1)	93.2600 (9)
F – M – F		75.0560 (2)	75.0559 (1)	75.0800 (9)	74.8175 (2)	74.8172 (0)	74.9200 (8)

The dynamic and static multipole deformation maps point out the convoluted and deconvoluted form of thermal contribution. The equation,characterizes the deformation densities of the maps, where $F_{multipole}$ represents the Fourier transform of the multipole charge density with or without the convolution of thermal contribution. Here, the fourier components are terminated at the experiment resolution.

"Atoms In Molecules (AIM) theory", proposed by Bader [44], facilitates the topology of electron density to provide a faithful documentation of the concept of atoms, bonds and structure, based on his quote, "two atoms are bonded if they are connected by a line of maximum electron density called a bond path, on which lies a bond critical point (BCP) where $\overrightarrow{\nabla}\rho(r_{BCP}) = 0$, and the critical points are the characteristics of the bond existing between the atoms".

3.2.2.2. Refinement. The refined structure factors from least-squares refinement were used for the multipole analysis for the core, valence and pseudo-atomic electron occupancies P_{lm} by using the software JANA 2006 [45]. The neutral atom wave functions are extracted from Clementi tables [46]. According to Hansen and Coppens [43], the slater type radial functions with $n_l = 4\ 4\ 6\ 8$ for Fe/Ga/Te and $n_l = 2\ 2\ 2\ 3$ for O/F, for $l \leq 4$ are used. During the refinement, the core charges for Fe/Ga, Te and O/F were taken as Kr, Xe and Ne respectively. For all these individual atoms, the valence expansion/contraction parameter (κ) is refined.

4. Data analysis

Bayesian statistical analysis was done to do away with experimental noise in the data. Further, as the electron density studies necessitate accurate structure factors, it is imperative that the efficacy of the refined structure factors is to be checked for systematic errors. The two benchmark tests of error analysis for the structure factors are to plot a histogram of the number of reflections against the function $[F_{MEM}(k)-F_{Obs}(k)]/\sigma(k)$ and an error map in the reciprocal lattice space. The distribution of the number of reflections and errors thus intrigued is presented as Fig. 2. The histogram reveals that the set of reflections with minimum $[F_{MEM}(k)-F_{Obs}(k)]/\sigma(k)$ are maximum and the values abide by a natural Gaussian distribution (Fig. 2(a) and (b)). Moreover, the error function distributed in reciprocal lattice space fluctuates between very small values (Fig. 2(c) and (d)). Both these checks disclose the fact that most of the reflections from the two data sets have the least possible errors. Consequently, these error tests exposed the quality of the data and the results obtained intimates a very good trend for the chosen statistical approach in understanding the crystallographic problems such as the charge density calculation.

5. Results and discussion

5.1. General structure properties, reliability indices and Debye-Waller factors

As already discussed, the structure refinement followed by MEM refinement have been carried out for the above said high quality single crystal data sets of both the oxyfluorotellurates and the results of these refinements are tabulated as Table 1. The geometrical results thus obtained from structure refinement are in excellent agreement with those obtained earlier [32]. The reliability indices are found to be 1.64% for Iron (III) Oxyfluorotellurate (IV) and 1.58% for Gallium (III) Oxyfluorotellurate (IV).

It is a universal truth that the vibration of the lighter atoms will be more when compared to that of the heavier atoms. Some of our own and other research works [47–50] have witnessed this fact while analyzing the Debye-Waller factors of the component atoms of the selected samples. In the present work also, in both the molecules, the thermal vibration factors of the constituent atoms act as a spectator of the above said fact. It is experimentally observed that the increasing trend of vibration is in the order: $Te < Fe/Ga < F < O$. While, regarding the oxygen atoms, it is noticed that, the atoms of different sites are vibrating with different amplitudes due to the different charge environment. In $FeTeO_3F$, the observed order is: $O3 > O2 > O1$, in contrast, in $GaTeO_3F$, the followed trend is $O2 > O3 > O1$. Furthermore, comparing the two compounds, the distorted coordination is more in Iron oxyfluorotellurate due to the fact that the atoms of the compound vibrate more vigorously than the counterpart in Gallium oxyfluorotellurate (Table 1). This kind of distorted coordination has already been found in several other family members. But is evidenced here experimentally. These evidences substantiate that Gallium oxyfluorotellurate has slightly larger binding force than Iron oxyfluorotellurate.

The MEM refinement parameters as given in Table 1 shows that the convergence criterion, C, tend to unity after 277 in $FeTeO_3F$ and 394 cycles in $GaTeO_3F$. The resolution of the maps constructed using maximum entropy method turn out to be 0.08 $e\text{Å}^{-3}$/pixel. The R factors are established as 1.46% for $FeTeO_3F$ and 1.08% for $GaTeO_3F$. Successful structure and MEM refinements and its resulting low residual factors impinge the meticulousness and high quality of the data once again and their service in calculating a clear-cut charge density in the unit cell.

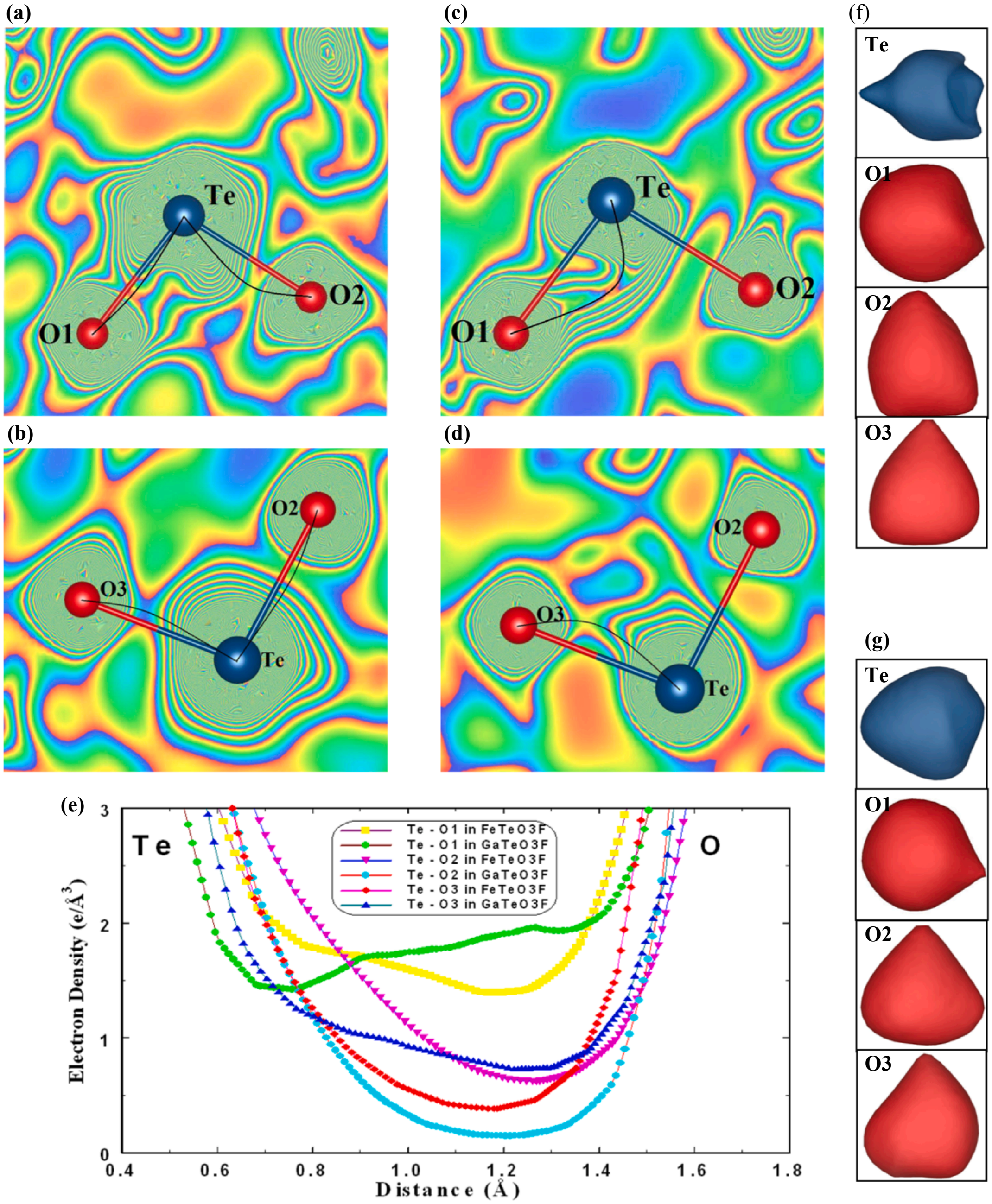

Fig. 4. Two-dimensional electron density maps of Te–O bonds in (a) and (b) $FeTeO_3F$ and (c) and (d) $GaTeO_3F$. (e) One dimensional charge density profiles of Te–O bonds. Atomic basins of (f) $FeTeO_3F$ and (g) $GaTeO_3F$.

5.2. Analysis of kappa refinement and deformation density maps

The multipole refinement implemented to the subjects of our study has furnished certain results which are presented as Table 2. A physically more acceptable description in Hansen and Coppens [43] model of multipole is that the refined values of κ and $\kappa^{'}$ authenticate the expansion of atoms, if it is less than 1 and contraction of atoms, if it is greater than 1. Anchored to this argument, the table clearly shows the signs of contraction of the tellurium and metal atoms in both the oxyfluorotellurates, since its κ values are greater than unity. Conversely, the ligand atoms are found to be expanding while bonding as its values are less than unity. Hence the two molecules display the same behavior in the course of expansion/contraction while bonding. However, the O2 atoms of both the compounds have distinctly expanded more than the atoms O1 and O3. This allows the distorted coordination in both the systems, while, once again it is found to be more in $FeTeO_3F$ than $GaTeO_3F$ since the expansion of O2 atom of the former is more than the latter. The values of core (P_c) and valance (P_v) charges of all the individual atoms mimic these effects. As an example, the sum of the Pc and P_v values of Te in $FeTeO_3F$ (51.0525) is less than its actual Z value (52) proves the contraction of that particular atom. The $\kappa^{'}$ that describes the expansion/contraction of the individual atoms could not be refined due to the fact that the highly reactive oxygen and fluorine ions occupy distorted territory which could not be exposed in smooth spherical boundaries.

The difference fourier maps constructed for $FeTeO_3F$ and $GaTeO_3F$ shown in Fig. 3(a) and (b) signify the less background density and noise, validating the enhanced quality of the data. To notice the effect of temperature on the charge distribution, the dynamic and static deformation maps are constructed (Fig. 3(c)–(f)) and these maps specify the

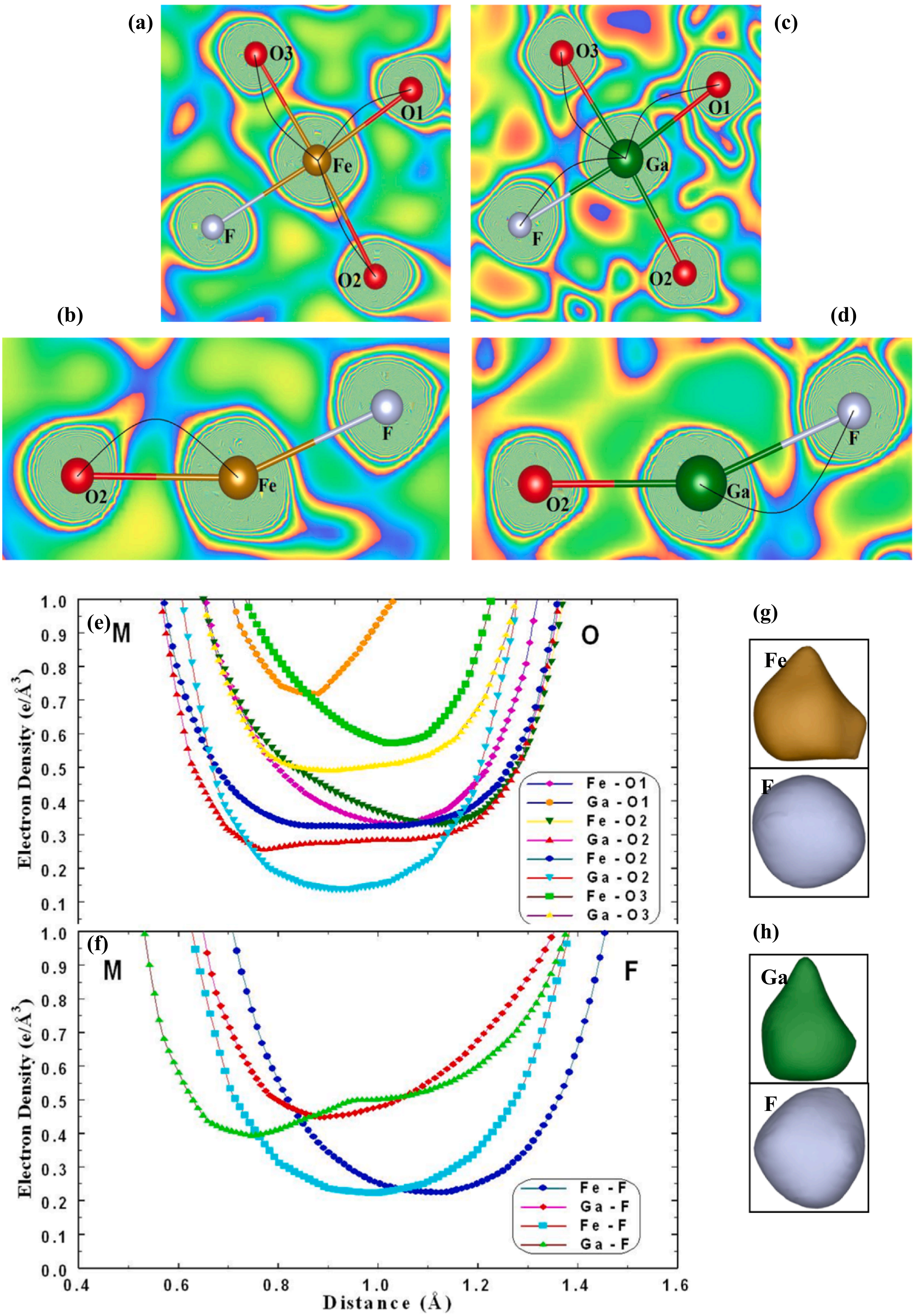

Fig. 5. Two-dimensional electron density maps of M − O/F bonds in (a) and (b) FeTeO$_3$F and (c) and (d) GaTeO$_3$F. One dimensional charge density profiles of (e) M − O bonds and (f) M − F bonds. Atomic basins of (g) FeTeO$_3$F and (h) GaTeO$_3$F.

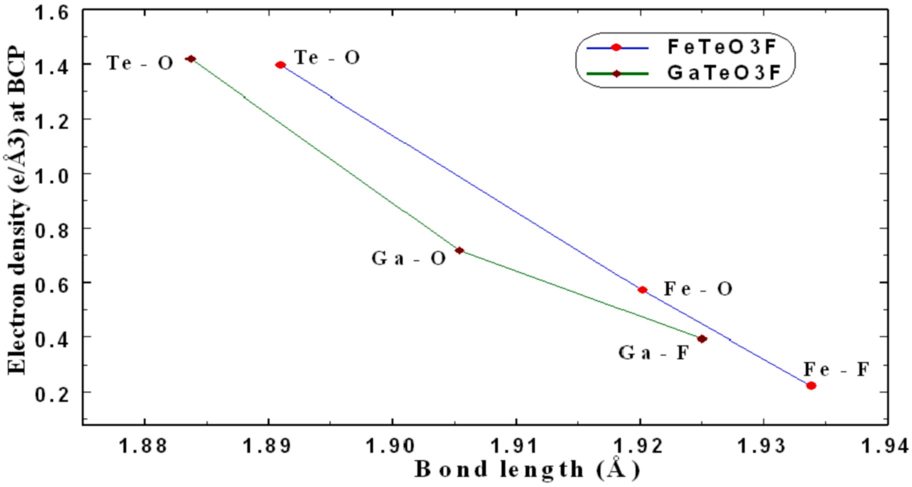

Fig. 6. Bond length versus Electron density at BCP.

Table 5
Atomic charges.

Atoms and parameters	Numerical integration			Least squares refinement	Numerical integration			Least squares refinement
	$FeTeO_3F$				$GaTeO_3F$			
	Q_{int}	Q_{eff}	Volume		Q_{int}	Q_{eff}	Volume	
Te	48.4969	3.5031	12.2204	–	45.5413	6.4587	12.0371	–
M	23.2142	2.7858	7.8776	–	26.2873	4.7127	7.5385	–
F	11.0881	−2.0881	14.5738	–	12.5334	−3.5334	13.9393	–
O1	10.3332	−2.3332	16.2167	–	11.7133	−3.7133	15.7600	–
O2	8.3430	−0.3430	12.8110	–	8.9531	−0.9530	12.6063	–
O3	9.5358	−1.5358	14.9874	–	10.9717	−2.9717	14.1741	–
Total charges in the unit cell	444.0448	–	–	444.0000	464.0004	–	–	464.0000
Total volume of the unit cell	–	–	314.7476	314.7200 (7)	–	–	304.2212	304.2200 (7)

less deformation of all the atoms. Moreover, the lone pair electrons of fluorine and oxygen atoms are obviously visible in the figures. Interestingly, perceiving Fig. 3(d) and (f), the lone pair orbitals of F and O3 atoms seem to interact with each other in $GaTeO_3F$.

5.3. *Characterization of bonding*

To unravel the features of charge densities in the bonding regions in crystal structures and to characterize the bonding between constituent atoms, two successful tracks have been used in this work. One is, mapping the 3-D and 2-D charge density distribution and 1-D charge density profiles, from which, a quantitative description as well as visualization of bonding features is accomplished. And the other one is, searching the (3,-1) bond critical points, in the places between every pair of neighboring nuclei using Newton-Raphson method, from which, a topological view of charge distribution pattern and quantitative explanation of the bonding mechanism is achieved. The bond lengths, bond angles and the amount of intermediate charges, measured by using these two paths are tabulated as Tables 3 and 4. The three dimensional arrangement of charges in the unit cell, elucidating the bonding electrons, are specified as Fig. 1 (b) and (c). The two dimensional miller planes, mapped to understand the bonding behavior between atoms are given as Figs. 4(a)–(d) and 5(a)–(d). For both the systems, the resolution of the maps turns out to be 0.08 $eÅ^{-3}$/pixel. One dimensional charge density profiles between the atoms, plotted to compute the bonding character are presented as Fig. 4 (e) and Fig. 5(e) and (f).

The 3-D MEM maps are sketched for the two systems, in ball and stick model of structure with isosurface level of 0.8 $e/Å^3$ (Fig. 1(b) and (c)). From the maps, the shapes and bondings between the constituent atoms and the valence charge density in real space are found to be well pronounced and clearly seen. In both the compounds, the most striking feature observed in the maps is the ligand atoms of different sites and also of the same site (O2) exhibit different bonding characteristics (depending on its symmetry). This effect is evidently visible in 2-D maps very clearly.

Undeniably, the two dimensional maps and one dimensional profiles are portrayals of Tables 3 and 4, i.e., the results obtained by using both the multipole and MEM methods. The bond lengths and bond angles obtained are compared with the reported ones in the tables. In Table 3, d, d_1 and d_2 signify the distances between Te/M atom – O/F atom, Te/M atom – CP (Critical Point) and CP–O/F atom correspondingly. According to Tsierelson [51], the density of charges at the BCP (Bond Critical Point) serves as a tool to characterize the interatomic interactions. As a consequent, the bondings between the atoms are typified as ionic interactions ($\rho\ (bcp) < 0.3$ $e/Å^3$), intermediate interactions ($0.3 < \rho\ (bcp) < 1$ $e/Å^3$) and polar covalent interactions ($1 < \rho\ (bcp) < 2\ e/Å^3$) [51–55]. In this regime, to give explicit effects to the visualization of the density variations in bonding regions and hence the regions turn out to be more visible and clear to categorize these interactions, the 2 – D maps are plotted in RGB (Red Green Blue) scale, in which the red shade in the saddle area indicates high density regions whereas the blue shade specify the low density regions. The curved bond paths are also specified in the figures.

Regarding the oxygen ligand, when it is binded to tellurium atoms, they exhibit various interaction types depending on its sites, in the two samples (Fig. 4). From Table 3, it is implicit that, in $FeTeO_3F$, O1 atom when bonded to Te atom, exhibit shared shell interaction as its ρ value is greater than unity (1.3952 $e/Å^3$), while O2 and O3 atoms, though its values of ρ are different (0.6175 $e/Å^3$ and 0.3838 $e/Å^3$ respectively), but less than unity, both the atoms exhibit intermediate interactions. In

$GaTeO_3F$, similar to $FeTeO_3F$, the O1 atom enacts shared shell interactions and O3 atom enacts intermediate interactions with tellurium atom. But, in contrary, the O2 atom exhibit closed shell interactions, when it is bonded to tellurium atom since it has a very low ρ value ($0.1467e/Å^3$). The red saddles between the lone pair cation and O1 in Fig. 4(a) and (c) substantiate the polar covalent interactions that exist in between these atoms in $FeTeO_3F$ and $GaTeO_3F$ respectively. The elongated saddles in 1-D profiles (Fig. 4(e)) also point out that the interactions between O1 and Te atoms are polar covalent in both the systems. The intermediate interactions are well pronounced through green shades between Te and O2 in $FeTeO_3F$ (Fig. 4(a) and (b)) and between Te and O3 in $GaTeO_3F$ (Fig. 4(d)) and blue shade (representing comparatively low density) between Te and O3 in $FeTeO_3F$ (Fig. 4(b)). The highly resolved O2 atom in Fig. 4(c) and (d) is an indication of ionic nature of bonding between Te and O2 in gallium oxyfluorotellurate. Moreover, Fig. 4(a) and (c) shows the distorted coordination in O1 – Te – O2. It can be substantiated by angles, distances and B_{iso} values (Tables 1, 3 and 4). These evidences make clear that the bonding between Te – O1 is very strong compared to O2. Comparing the Debye-Waller factors of these ligands, O2 has a larger B_{iso} value than the other. Hence it is evident that mostly O2 and the type of bonding between Te and O2 actually make the coordination as distorted.

Andrew G.Christy and Stuart J.Mills [56] have underestimated the conventional electron density maps that they are inadequate to visualize and distinguish the lone pairs. On the contrary, Fig. 4(a) and (c) obviously show the lone pair electrons as small dense and well localized cap of non – bonding electrons that is concave upwards over the tellurium atom. As calculated by Galy et al. [57], the distance between the Te^{IV} cation and the lone electron pairs is 1.25 Å. Close to this argument, from the MEM maps, the L – E distances are found to be 1.3144 Å in $FeTeO_3F$ and 1.2778 Å in $GaTeO_3F$.

Considering the bonding between the oxygen ligand of three different sites and the metal cation, the interaction types differs depending on the site as well as the symmetry of the ligand (Fig. 5). In iron oxyfluorotellurate, even though the electron densities at the critical points of the Fe–O bonds differs (Table 3), all the interactions are of intermediate type. But in case of gallium oxyfluorotellurate, the ligands O1 and O3 when bonded to Ga atom exhibit intermediate characteristics, but the ligand atoms O2, at two different symmetries, when bonded to the same Ga atom exhibit closed shell interactions, as the electron densities at the critical points are very low. And also, in both the molecules, inspite of the dissimilar symmetries of two O2 atoms, the interaction kinds are same with slight difference in bond length as well as ρ values. Fig. 5(a), (b) and (c) showing green and blue shades in the bonding regions between Fe/Ga and O (except between Ga and O2) indicating intermediate interactions and Fig. 5(c) and (d) showing well resolved electron clouds around O2 in the molecule $GaTeO_3F$ signifying ionic interactions, are strong evidences of Table 3. The one dimensional plots drawn (Fig. 5(e)) once again confirm these results. Analogous to the DMD and SMD maps of $GaTeO_3F$, the mem maps also shows the interactions between the lone pair electron orbitals of F and O3 atom (Fig. 5(c)). Searching for the same kind of interaction in $FeTeO_3F$ proved futile. Hence it can be understood that these interactions in $GaTeO_3F$ makes the system harder than the other. It may also be attributed to the distorted coordination in $FeTeO_3F$ that makes the system fragile than the other.

In view of the fluorine ligand, the atoms display completely different bonding categories in the two compounds (Fig. 5). In $FeTeO_3F$, the bonding between the metal cation and fluorine atoms at both the symmetries (-x, -y,- z) and (x, y, z) are predominantly ionic as the charge densities at the bond critical points are 0.2246 Å and 0.2224 Å respectively, while, in $GaTeO_3F$, the same between Ga and F at symmetries (-x, -y,- z) and (x, y, z) are intermediate as the values of ρ at the bond critical points are 0.4486 Å and 0.3939 Å respectively. The well resolved F atoms in Fig. 5(a) and (b), blue saddles between Ga atom and F atoms in Fig. 5 (c) and (d) and the 1–D mem profiles (Fig. 5(f)) authenticates our outcomes in Table 3.

This complete and well documented topological analysis done by using two methods validates a mixed ionic and covalent type of bonding existing in the two samples. Hence for a more apparent construal, the bond length is plotted against the electron density at bcp (Fig. 6). The most common and familiar fact about bonds is that, the shortest bond is the best possible bond within the unit cell, owing to its perfect geometrical arrangement of charges in that bonds. Consequently, the shortest bond in each kind, i.e., Te–O, M – O and M – F, is taken in to account. Figure shows that, in both the compounds, the shortest bonds are the strongest i.e., polar covalent, and as the length ascends, the strength of the bond descends, i.e., the density of charges at the critical point of the bonds descends and ultimately the weak bonds are ionic in nature. As suggested by Nenian Charles et al. [13] and Yu. A.Hizhnyi e.al [21], in both the systems, the M – O bonds are less ionic with shorter bond lengths compared to the longer M – F bonds. Significantly, comparing the two systems, all the three bonds (Te–O, M – O and M – F) are stronger in $GaTeO_3F$ than $FeTeO_3F$. This reflects the results offered by Debye-Waller factors in Table 1. And also the bonds of $GaTeO_3F$ have more covalent nature than those of $FeTeO_3F$. That finalized the argument that $GaTeO_3F$ is harder as a material than $FeTeO_3F$.

5.4. *Atomic basins and charges*

For a close and clear visualization of the spherical and aspherical nature of individual atoms and to calculate the integrated charges, the true valence charge density surfaces are drawn (Figs. 4(f) and (g), 5(g) and 5(h)) by identifying zero flux surface (ZFS) at all directions which encapsulates the atomic basins, i.e, regions of space, traversed by trajectories of the density gradient termination at a given nucleus which is enclosed inside a zero charge density flux surface $\vec{\nabla}\rho \, . \, \vec{n}$, where $\vec{n}$ is the unit vector of surface. Pertaining to our previous work [55], the figures of atomic basins reveals that the symmetries and bonding natures of the atoms have no effect on the atomic basins, and apparently, the site of that particular atom matters. And also, the figures of the basins of F atoms are close to spherical shape. Fascinatingly, the shapes of basins of the constituent atoms in $FeTeO_3F$ and $GaTeO_3F$ roughly imitate each other.

Electron densities at BCPs together with the quantified transfer of charge are well capable to provide a lucid description of bonding features. Hence, in the both the molecules, the atomic charges are calculated by using the method of numerical integration of the charge density over zero flux atomic basins and tabulated as Table 5. The table implies that the charges transferred from Te atom to the three oxygen atoms O1, O2 and O3 atoms, in $FeTeO_3F$ is 3.5031e, and while in $GaTeO_3F$ is 6.4587e. And also, a transfer of 2.7858e from Fe atom the two F and the four oxygen atoms (one O1, two O2 and one O3 atom): 1.0441e are transferred to each F atom, while the remaining 0.6977e is associated to the four oxygen atoms, is found in iron oxyflurotellurate. In case of gallium oxyflurotellurate, a transfer of 4.7127e from gallium atom to the two fluorine atoms and four oxygen atoms (one O1, two O2 and one O3 atom): 1.7667e is associated to each fluorine atom, while the remaining 1.1793e are transferred to the four oxygen atoms is found.

In fact, the atomic basins of atoms, which have high electronegative character, occupy larger atomic basin volume. Confirming this argument, ligand atoms, fluorine and oxygen having high electronegative character of about 3.98 and 3.44 correspondingly, were found to occupy larger atomic basin volumes than the other two cations (Te and Fe/Ga) in both the systems. Comparing tellurium and metal atoms, as the electronegativity of Te ($\chi = 2.1$) is slightly larger than Fe ($\chi = 1.83$) and Ga ($\chi = 1.81$), the volume of atomic basins of tellurium is larger than that of iron and gallium. All these informations are evidently visible in the drawn atomic basins presented as Fig. 4(f) and (g), 5(g) and 5(h). Moreover, the table shows that the total charges in one unit cell of $GaTeO_3F$ is more than that in one unit cell of $FeTeO_3F$, but the volume of the unit cell of $GaTeO_3F$ is less than that of $FeTeO_3F$. This discloses that the unit cell of gallium oxyfluorotellurate is closely packed whereas that of iron oxyfluorotellurate is loosely packed.

Hence, scrutinizing the present work of charge density estimation on the oxyfluorotellurates of iron and gallium, it is concluded that $GaTeO_3F$ is more rigid and FeTeO3F is fragile. Perhaps, the dense packing of atoms in the unit cell of the former and the slackly packing nature of the latter forms the basis of the above supposed argument. Between these two systems, it is experimentally found that $GaTeO_3F$ contains more covalent character than $FeTeO_3F$.

6. Conclusion

The present charge density work of the two oxyfluorotellurates has given ample information on the nature of bonding between its constituent atoms and the amount of integrated charges which is very useful in understanding the properties of the chosen materials. The expansion/contraction and vibration of individual atoms are analyzed in detail. Electron densities along different bonding planes are validated qualitatively as well as quantitatively. Our conclusions from this investigation are that, gallium oxyfluorotellurate is a hard molecule than iron oxyfluorotellurate. And also, $GaTeO_3F$ has more covalent nature of bonding than $FeTeO_3F$. Same sort of investigation in more oxyfluorides comprising lone pair cations would enhance the knowledge about their bonding and electronic structures and open up the possibility of tuning their properties, which is essential for various technological applications in future.

Declaration of competing interest

There is no conflict of interest between me and any other party.

References

[1] M. Eckert, Disputed discovery: the beginnings of X-ray diffraction in crystals in 1912 and its repercussions, Acta Crystallogr. A 68 (2012) 30–39.

[2] H. Toraya, 100-Year anniversary of X-ray crystallography, Rigaku Journal 30(2) (2014).

[3] S. Tibor, Koritsanszky, Philip Coppens, Chemical applications of X-ray charge-density analysis, Chem. Rev. 101 (2001) 1583–1627.

[4] G.U. Kulkarni, R.S. Gopalan, C.N.R. Rao, Experimental and theoretical electronic charge densities in molecular crystals, J. Mol. Struct. 500 (2000) 339–362.

[5] R. Saravanan, M. Prema Rani, Metal and alloy bonding: an experimental analysis, Springer-Verlag London Ltd. (2012).

[6] R.Barron Andrew, Compounds of flourine, OpenStax-CNX module: m33815 (2010) 1–4.

[7] E.Henrich Victor, Metal Oxide Surfaces and Interfaces: Concepts and Issues", Book – "The Chemical Physics of Solid Surfaces : Oxide Surfaces, vol. 9, Elsevier Science, 2001.

[8] C.N.R. Rao, II. Transition metal oxides (including cuprate superconductors), Annu. Rev. Phys. Chem. 40 (1989) 291–326.

[9] Gabriele Centi, Fabrizio Cavani, Ferrucio Trifiro, selective oxidation by heterogeneous catalysis, Springer Sci. Bus. media (2012).

[10] B.L. Chamberland, "The Crystal Chemistry of Transition Metal Oxyfluorides", Book – "Inorganic Solid Fluorides Chemistry and Physics", Academic Press, Inc, 1985.

[11] J. Ravez, The inorganic fluoride and oxyfluoride ferroelectrics, J Phys. III France 7 (1997), 1129 – 1144.

[12] Vincent L. Chevrier, Geoffroy Hautier, Shyue Ping Ong, Robert E. Doe, Gerbrand Ceder, First – principles study of iron oxyfluorides and lithiation of FeOF, Phys. Rev. B 87 (2013) 094118–094119, 094118-1 &ndash.

[13] Nenian Charles, James M. Rondinelli, Assessing exchange – correlation functional performance for structure and property predictions of oxyfluoride compounds from first principles, Physical Rev. B 94 (2016), 174108-1-174108-15.

[14] Masayuki Takashima, Gentaro Kanoh, Preparation of rare earth oxyfluorides and their properties as a material for fuel cell, J. Fluorine Chem. Volume 21 (Issue 1) (1982) 16.

[15] P. Shiv Halasyamani, Noncentrosymmetric Inorganic Oxide Materials: Synthetic Strategies and Characterisation Techniques", Book – "Inorganic Materials Series Functional Oxides, A John Wiley and sons, Ltd, Publication, 2010.

[16] Shinobu Fujihara, Takayoshi Kato, Toshio Kimura, Sol – gel processing and luminescent properties of rare – earth oxyfluoride materials, J. sol – gel Sci. Technol. 26 (2003) 953–956.

[17] V. Maxim, Lobanov, A.M. Abakumov, A.V. Sidorova, M.G. Rozova, O. G Dyachenko, E.V. Antipov, J. Hadermann, G. Van Tendeloo, Synthesis and investigation of novel Mn-based oxyfluoride $Sr_2Mn_2O_{5-x}F_{1+x}$, Solid State Sci. 4 (2002) 19–22.

[18] M. Corey, Thompson, Colin K. Blakely, Roxana Flacau, John E. Greedan, Viktor V. Poltavets, Structural and magnetic behavior of the cubic oxyfluoride SrFeO2F studied by neutron diffraction, J. solid state Chem. 219 (2014) 173–178.

[19] D. Deng, Transition metal oxyfluorides for next – generation rechargeable batteries, ChemNanoMat 3 (Issue 3) (2016).

[20] Li Liu, Xianyou Wang, Xingyan Wang, Xin Wang, Fanghua Tian, Yi Lanhua, Synthesis and electrochemical performance of bismuth – vanadium oxyfluoride, Electrochim. Acta 56 (2011) 7437–7441.

[21] Yu, A. Hizhnyi, S.G. Nedilko, V.P. Chornii, T.M. Nikolaenko, N.S. Slobodyanik, V. I. Sheludko, Structure of the fluorine states in cadmium molybdate host studied by the electronic band structure calculations of $CdMoO_4$, $CdMoO_4$:F and $CdMoO_3F_2$ crystals, Comput. Mater. Sci. 87 (2014) 12–18.

[22] E. Melnichenko, O. Gorbenko, N. Laptash, S. Polyshchuk, Solid transition metal oxyfluorides, J. Fluorine Chem. Volume 45 (Issue 1) (1989) 52.

[23] A.G. Christy, S.J. Mills, A.R. Kampf, A review of the structural architecture of tellurium oxycompounds, Mineral. Mag. Volume 80 (3) (2016) 415–545.

[24] S. Imran Ali, R. K Kremer, M. Johnsson, Hydrothermal synthesis of the oxofluoride $FeSbO_2F_2$ – an anti-ferromagnetic spin $S = 5/2$ compound, American Chemical Society, Inorg. Chem. 56 (2017) 4662–4667.

[25] Sk Imran Ali, Weiguo Zhang, Shiv Halasyamani, Mats Johnsson, $Zn_3Sb_4O_6F_6$: hydrothermal synthesis, crystal structure and nonlinear optical properties, J. solid state Chem. 256 (2017) 158–161.

[26] S. Hu, M. Johnsson, Synthesis and crystal structure of two synthetic oxofluoride framework compounds - $Co_2TeO_3F_2$ and $Co_2SeO_3F_2$, Dalton Trans. 41 (2012) 12786–12789.

[27] Shichao Hu, Mats Johnsson, M.Law Joseph, Jerry L. Bettis Jr., Myung-Hwan Whangbo, K. Reinhard, Kremer, Crystal structure and magnetic properties of $FeSeO_3F$ – alternating antiferromagnetic $S = 5/2$ chains, Am. Chem. Soc., Inorg. Chem. 53 (2014) 4250–4256.

[28] Jean Paul Laval, Nefla Jennene Boukharrata, New vanadium(IV) and titanium(IV) oxyfluorotellurates(IV): V2Te2O7F2 and TiTeO3F2, Acta Crystallogr. C C65 (2009) i1–16.

[29] N. Jennene Boukharrata, J.P. Laval, Synthesis and structure determination of $In_3TeO_3F_7$: an indium oxyfluorotellurate IV derived from W bronze structure with Te^{4+} in hexagonal tunnels, J. Alloy. comp. 509 (2011) 1517–1522.

[30] Nefla Jennene Boukharrata, Jean-Rene Duclere, Jean Paul Laval, Philippe Thomas, A new oxyfluorotellurate (IV), InTe2O5F, Acta Crystallogr. C C69 (2013) 1–3.

[31] Nefla Jennene Boukharrata, Jean Paul Laval, Philippe Thomas, Two new types of oxyfluorotellurates (IV): ScTeO3F and InTeO3F, Acta Crystallogr. C C64 (2013) i57–i61.

[32] Jean Paul Laval, Nefla Jennene Boukharrata, Philippe Thomas, New oxyfluorotellurates (IV): MTeO3F (M = FeIII, GaIII and CrIII, Acta Crystallogr. C C64 (2008) i12–i14.

[33] M. Artem, Abakumov, Dmitry Batuk, A.Tsirlin Alexander, ClemensPrescher, Leonid Dubrovinsky, Denis V. Sheptyakov, Walter Schnelle, Joke Hadermann, Gustaaf Van Tendeloo, Frustrated pentagonal cairo lattice in the non-collinear antiferromagnet $Bi_4Fe_5O_{13}F$, Physical Rev. B87 (2013), 024423-1-024423-9.

[34] Yoshiyuki Inaguma, Jean-Marc Greneche, Marie-Pierre Crosnier-Lopez, Tetsuhiro Katsumata, Yvon Calage, Jean-Louis Fourquet, "Structure and Mossbauer studies of F – O ordering in antiferromagnetic perovskite $PbFeO_2F$", American Chemical Society, Chem. Mater. 17 (2005) 1386–1390.

[35] J.-H. Feng, C.-L. Hu, H.-P. Xia, F. Kong, J.-G. Mao, $Li_7(TeO_3)_3F$: a lithium fluoride tellurite with large second harmonic generation responses and a short ultraviolet cutoff edge, Am. Chem. Soc., Inorg. Chem. Volume 56 (23) (2017) 14697–14705.

[36] International Tables for X-ray Crystallography, Vol. IV, (The Kynoch Press, England, 1974).

[37] W.H. Zachariasen, Acta Crystallogr. 23 (1967) 558.

[38] M. Collins, Nature 298 (1982) 49.

[39] M. Sakata, M. Sato, Acta Cryst. A46 (1990) 263.

[40] R.A. Dilanian, F. Izumi, Super-fast Program, PRIMA, for the Maximum Entropy Method, 2005.

[41] F. Izumi, R.A. Dilanian, Part II, Recent Research Developments in Physics, vol. 3, Transworld Research Network, Trivandrum, 2002, p. 699.

[42] K. Momma, F. Izumi, VESTA, Visualisation for electronic and structual analysis, Comm. Crystallogr. Comput., IUCr Newslett. 7 (2006) 106.

[43] N.K. Hansen, P. Coppens, Acta Crystallogr. A34 (1978) 909–921.

[44] R.F.W. Bader, Atoms in Molecules—A Quantum Theory, Oxford Univ. Press, Oxford, 1990.

[45] V. Petricek, M. Dusek, L. Palatinus, JANA, The crystallographic computing system, Institute of Physics, Acad. sci. Czech republic Praha (2006), 2000.

[46] E. Clementi, C. Roetti, Roothaan-Hatree-Fock atomic wave functions, At. Data Nucl. Tables 14 (1974) 177–478.

[47] S. Israel, R. Saravanan, R.K. Rajaram, Electronic structure of InP at RT, 200 and 100 K, Physica B 349 (2004) 390–400.

[48] R. Saravanan, M. Prema Rani, Bonding in CoAl and NiAl metal alloys using multipole and MEM techniques, J. Alloy. Comp. 431 (2007) 121–129.

[49] S. Israel, K.S. Syed Ali, R.A.J.R. Sheeba, R. Saravanan, X-ray analysis of the charge density distribution in GaP at 296 and 200 K using a multipole model and the maximum entropy method, Chin. J. Phys. 47 (No. 3) (2009) 378–400.

[50] K. Sujatha, S. Israel, C. Anzline, R. Niranjana Devi, R.A.J.R. Sheeba, X-ray derived experimental charge density distribution in GaF_3 and VF_3 solid systems, Physica B 496 (2016) 74–81.

[51] V.G. Tsierelson, Acta Crystallogr. A55 (1999) Supplement, Abstract M 13-OF-003, 1999.

[52] I. Adam, Stash, Tanaka Kiyoaki, Kazunari Shiozawa, Hitoshi Makino, Vladimir G. Tsirelson, Atomic interactions in ethylenebis (1-indenyl) zirconium dichloride as derived by experimental electron density analysis, Acta Cryst B61 (2005) 418–428.

[53] S. Israel, K.S. Syed Ali, R.A.J.R. Sheeba, R. Saravanan, Analysis on experimental valence charge density in germanium at RT and 200K, J. Phy. Chem. solids 70 (2009) 1185–1194.

[54] S. Israel, K.S. Syed Ali, R.A.J.R. Sheeba, R. Saravanan, X-ray analysis of the charge density distribution in GaP at 296 and 200K using a multipole model and the maximum entropy method", Chin. J. Phys. 47 (No.3) (2009) 378–400.

[55] K. Sujatha, S. Israel, C. Anzline, K.S. Syed Ali, R.A.J.R. Sheeba, P. Richard Rajkumar, Analysis of Oxygen bonding with metals of different oxidation states from experimental charge density distribution, Physica B 555 (2019) 21–31.

[56] G. Andrew, Christy, J.Mills Stuart, Effect of lone-pair stereoactivity on polyhedral volume and structural flexibility: application to $Te^{IV}O_6$ octahedra, Acta Crystallogr. Sect. B, Struct. sci. Crystal Eng. Mater. B69 (2013) 446–456.

[57] J. Galy, G. Meunier, S. Andersson, A.J. Astrom, Stereochemistry of Elements with Unbound Pairs; Ge(II), As(III), Se(IV), Br(V), Sn(II), Sb(III), Te(IV), I(V), Xe(VI), Tl (I), Pb(II), and Bi(III) (Oxides, Fluorides and Oxyfluorides), J. Solid State Chem. vol. 13 (1975) 142–159.